

Observation of $B \rightarrow K_S^0 \pi^+ \pi^-$ and Evidence for $B \rightarrow K^{*\pm} \pi^\mp$

CLEO Collaboration

(December 3, 2002)

Abstract

We report on a search for charmless hadronic B decays to the three-body final states $K_S^0 h^+ \pi^-$, $K^+ h^- \pi^0$, $K_S^0 h^+ \pi^0$ (h^\pm denotes a charged pion or kaon), and their charge conjugates, using 13.5 fb^{-1} of integrated luminosity produced near $\sqrt{s} = 10.6 \text{ GeV}$, and collected with the CLEO detector. We observe the decay $B \rightarrow K^0 \pi^+ \pi^-$ with a branching fraction $(50_{-9}^{+10}(\text{stat.}) \pm 7(\text{syst.})) \times 10^{-6}$ and the decay $B \rightarrow K^{*+}(892) \pi^-$ with a branching fraction $(16_{-5}^{+6}(\text{stat.}) \pm 2(\text{syst.})) \times 10^{-6}$.

E. Eckhart,¹ K. K. Gan,¹ C. Gwon,¹ T. Hart,¹ K. Honscheid,¹ D. Hufnagel,¹ H. Kagan,¹
R. Kass,¹ T. K. Pedlar,¹ J. B. Thayer,¹ E. von Toerne,¹ T. Wilksen,¹ M. M. Zoeller,¹
H. Muramatsu,² S. J. Richichi,² H. Severini,² P. Skubic,² S.A. Dytman,³ J.A. Mueller,³
S. Nam,³ V. Savinov,³ S. Chen,⁴ J. W. Hinson,⁴ J. Lee,⁴ D. H. Miller,⁴ V. Pavlunin,⁴
E. I. Shibata,⁴ I. P. J. Shipsey,⁴ D. Cronin-Hennessy,⁵ A.L. Lyon,⁵ C. S. Park,⁵ W. Park,⁵
E. H. Thorndike,⁵ T. E. Coan,⁶ Y. S. Gao,⁶ F. Liu,⁶ Y. Maravin,⁶ R. Stroynowski,⁶
M. Artuso,⁷ C. Boulahouache,⁷ K. Bukin,⁷ E. Dambasuren,⁷ K. Khroustalev,⁷
R. Mountain,⁷ R. Nandakumar,⁷ T. Skwarnicki,⁷ S. Stone,⁷ J.C. Wang,⁷ A. H. Mahmood,⁸
S. E. Csorna,⁹ I. Danko,⁹ G. Bonvicini,¹⁰ D. Cinabro,¹⁰ M. Dubrovin,¹⁰ S. McGee,¹⁰
A. Bornheim,¹¹ E. Lipeles,¹¹ S. P. Pappas,¹¹ A. Shapiro,¹¹ W. M. Sun,¹¹ A. J. Weinstein,¹¹
F. Würthwein,^{11,*} R. Mahapatra,¹² R. A. Briere,¹³ G. P. Chen,¹³ T. Ferguson,¹³
G. Tatishvili,¹³ H. Vogel,¹³ N. E. Adam,¹⁴ J. P. Alexander,¹⁴ K. Berkelman,¹⁴ V. Boisvert,¹⁴
D. G. Cassel,¹⁴ P. S. Drell,¹⁴ J. E. Duboscq,¹⁴ K. M. Ecklund,¹⁴ R. Ehrlich,¹⁴ L. Gibbons,¹⁴
B. Gittelman,¹⁴ S. W. Gray,¹⁴ D. L. Hartill,¹⁴ B. K. Heltsley,¹⁴ L. Hsu,¹⁴ C. D. Jones,¹⁴
J. Kandaswamy,¹⁴ D. L. Kreinick,¹⁴ A. Magerkurth,¹⁴ H. Mahlke-Krüger,¹⁴ T. O. Meyer,¹⁴
N. B. Mistry,¹⁴ E. Nordberg,¹⁴ J. R. Patterson,¹⁴ D. Peterson,¹⁴ J. Pivarski,¹⁴ D. Riley,¹⁴
A. J. Sadoff,¹⁴ H. Schwarthoff,¹⁴ M. R. Shepherd,¹⁴ J. G. Thayer,¹⁴ D. Urner,¹⁴
B. Valant-Spaight,¹⁴ G. Viehhauser,¹⁴ A. Warburton,¹⁴ M. Weinberger,¹⁴ S. B. Athar,¹⁵
P. Avery,¹⁵ L. Brevi-Newell,¹⁵ V. Potlia,¹⁵ H. Stoeck,¹⁵ J. Yelton,¹⁵ G. Brandenburg,¹⁶
D. Y.-J. Kim,¹⁶ R. Wilson,¹⁶ K. Benslama,¹⁷ B. I. Eisenstein,¹⁷ J. Ernst,¹⁷ G. D. Gollin,¹⁷
R. M. Hans,¹⁷ I. Karliner,¹⁷ N. Lowrey,¹⁷ M. A. Marsh,¹⁷ C. Plager,¹⁷ C. Sedlack,¹⁷
M. Selen,¹⁷ J. J. Thaler,¹⁷ J. Williams,¹⁷ K. W. Edwards,¹⁸ R. Ammar,¹⁹ D. Besson,¹⁹
X. Zhao,¹⁹ S. Anderson,²⁰ V. V. Frolov,²⁰ Y. Kubota,²⁰ S. J. Lee,²⁰ S. Z. Li,²⁰ R. Poling,²⁰
A. Smith,²⁰ C. J. Stepaniak,²⁰ J. Urheim,²⁰ Z. Metreveli,²¹ K.K. Seth,²¹ A. Tomaradze,²¹
P. Zweber,²¹ S. Ahmed,²² M. S. Alam,²² L. Jian,²² M. Saleem,²² and F. Wappler²²

¹Ohio State University, Columbus, Ohio 43210

²University of Oklahoma, Norman, Oklahoma 73019

³University of Pittsburgh, Pittsburgh, Pennsylvania 15260

⁴Purdue University, West Lafayette, Indiana 47907

⁵University of Rochester, Rochester, New York 14627

⁶Southern Methodist University, Dallas, Texas 75275

⁷Syracuse University, Syracuse, New York 13244

⁸University of Texas - Pan American, Edinburg, Texas 78539

⁹Vanderbilt University, Nashville, Tennessee 37235

¹⁰Wayne State University, Detroit, Michigan 48202

¹¹California Institute of Technology, Pasadena, California 91125

¹²University of California, Santa Barbara, California 93106

¹³Carnegie Mellon University, Pittsburgh, Pennsylvania 15213

¹⁴Cornell University, Ithaca, New York 14853

¹⁵University of Florida, Gainesville, Florida 32611

¹⁶Harvard University, Cambridge, Massachusetts 02138

*Permanent address: Massachusetts Institute of Technology, Cambridge, MA 02139.

¹⁷University of Illinois, Urbana-Champaign, Illinois 61801

¹⁸Carleton University, Ottawa, Ontario, Canada K1S 5B6
and the Institute of Particle Physics, Canada M5S 1A7

¹⁹University of Kansas, Lawrence, Kansas 66045

²⁰University of Minnesota, Minneapolis, Minnesota 55455

²¹Northwestern University, Evanston, Illinois 60208

²²State University of New York at Albany, Albany, New York 12222

Recent years have seen [1] the first observations of several two-body charmless hadronic decays of B mesons, including the four $B \rightarrow K\pi$ transitions. These two-pseudoscalar decays have received considerable attention due to their expected role in improving our understanding of the weak interaction and in the extraction of the complex quark couplings described by the Cabibbo-Kobayashi-Maskawa matrix [2]. The pseudoscalar-vector analogs of these decays, $B \rightarrow K^*\pi$ and $K\rho$, provide further constraints on the magnitudes and phases of these couplings and present additional opportunities for observing direct CP violation [3] and deviations from the Standard Model. Accurate measurement and interpretation of the rates and CP asymmetries of these quasi-two-body decays requires knowledge of the non-resonant contributions to the same final states [4]. In this Letter, we report on a study of B decays to the three-pseudoscalar final states, $K_S^0 h^+ \pi^-$, $K^+ h^- \pi^0$, and $K_S^0 h^+ \pi^0$ (h^\pm denotes a charged pion or kaon), without regard for the resonant substructure. For each final state, we also search for two-body channels with intermediate vector resonances, as well as for non-resonant production. Results for the $K_S^0 h^+ \pi^-$ and $K^+ h^- \pi^0$ topologies have been presented previously by the CLEO [5] and Belle [6] Collaborations. The inclusion of charge conjugate states is always implied.

The data sample used in this analysis was produced in symmetric e^+e^- collisions at the Cornell Electron Storage Ring (CESR) and collected with the CLEO detector in two configurations, known as CLEO II [7] and CLEO II.V [8]. It comprises 9.12 fb^{-1} of integrated luminosity collected on the $\Upsilon(4S)$ resonance, corresponding to 9.7×10^6 $B\bar{B}$ pairs, of which 6.3×10^6 were taken with CLEO II.V. An additional 4.36 fb^{-1} collected below the $B\bar{B}$ production threshold is used to study non- $B\bar{B}$ backgrounds. The response of the experimental apparatus is studied with a GEANT-based [9] simulation of the CLEO detector, where the simulated events are processed in a fashion similar to data.

In CLEO II, the momenta of charged particles are measured with a tracking system consisting of a six-layer straw tube chamber, a ten-layer precision drift chamber, and a 51-layer main drift chamber, all operating inside a 1.5 T superconducting solenoid. The main drift chamber also provides a measurement of specific ionization energy loss (dE/dx), which is used for particle identification. For CLEO II.V, the six-layer straw tube chamber was replaced by a three-layer double-sided silicon vertex detector, and the gas in the main drift chamber was changed from an argon-ethane to a helium-propane mixture. Photons are detected with a 7800-crystal CsI electromagnetic calorimeter, which is also inside the solenoid. Proportional chambers placed at various depths within the steel return yoke of the magnet identify muons.

Charged tracks are required to be well-measured and to satisfy criteria based on the track fit quality and must be consistent with coming from the interaction point in three dimensions. Pions and kaons are identified by dE/dx , and tracks that are positively identified as electrons or muons are not allowed to form the B candidate. We form π^0 candidates from pairs of photons with an invariant mass within $20 \text{ MeV}/c^2$ or approximately 2.5 standard deviations (σ) of the known π^0 mass. These are then kinematically fitted with the mass constrained to the known π^0 mass. We also require the π^0 momentum to be greater than $1 \text{ GeV}/c$ to reduce combinatoric background from low-momentum π^0 candidates. K_S^0 candidates are selected from pairs of tracks with invariant mass within $10 \text{ MeV}/c^2$ or 2.5σ of the known K_S^0 mass. In addition, K_S^0 candidates are required to originate from the beam spot and to have well-measured displaced decay vertices.

We identify B meson candidates by their invariant mass and the total energy of their decay products. We calculate a beam-constrained mass by substituting the beam energy (E_b) for the measured B candidate energy: $M \equiv \sqrt{E_b^2 - \mathbf{p}_B^2}$, where \mathbf{p}_B is the B candidate momentum. Performing this substitution improves the resolution of M by one order of magnitude, to about 3 MeV/ c^2 . We define $\Delta E \equiv E_1 + E_2 + E_3 - E_b$, where E_1 , E_2 , and E_3 are the energies of the B candidate daughters. For final states with a K_S^0 and two charged tracks, the ΔE resolution is about 20 MeV for CLEO II and 15 MeV for CLEO II.V. A π^0 in the final state degrades this resolution by approximately a factor of two. ΔE is always calculated assuming the h^\pm is a pion. Therefore, the ΔE distribution for pions is centered at zero, while that for kaons is shifted by at least -40 MeV. We accept B candidates with M between 5.2 and 5.3 GeV/ c^2 and with $|\Delta E|$ less than 300 MeV for modes containing a π^0 and 200 MeV for $K_S^0 h^+ \pi^-$. This region includes the signal region and a generous sideband for background normalization. We reject candidates that are consistent with the exclusive $b \rightarrow c$ transitions $B \rightarrow D\pi$, where $D \rightarrow K\pi$, and $B \rightarrow \psi K^0$, where $\psi \rightarrow \mu^+ \mu^-$ and the muons are misidentified as pions.

The main background in this analysis arises from $e^+e^- \rightarrow q\bar{q}$, where $q = u, d, s, c$. To suppress this background, we calculate the angle θ_{sph} between the sphericity axis [10] of the tracks and showers forming the B candidate and that of the remainder of the event. Because of their two-jet structure, continuum $q\bar{q}$ events peak strongly at $|\cos \theta_{\text{sph}}| = 1$, while the more isotropic $B\bar{B}$ events are nearly flat in this variable. By requiring $|\cos \theta_{\text{sph}}| < 0.8$, we reject 83% of the continuum background while retaining roughly the same fraction of signal B decays. Additional separation of signal from $q\bar{q}$ background is provided by a Fisher discriminant [11] \mathcal{F} formed from eleven variables: the angle between the sphericity axis of the candidate and the beam axis, the ratio of Fox-Wolfram moments H_2/H_0 [12], and the scalar sum of the visible momentum in nine 10° angular bins around the candidate sphericity axis. We also make use of the angle between the B candidate momentum and the beam axis, θ_B . Angular momentum conservation causes B mesons produced through the $\Upsilon(4S)$ to exhibit a $\sin^2 \theta_B$ dependence, while candidates from continuum are flat in $\cos \theta_B$.

Our loose selection criteria result in samples consisting primarily of background events and containing 11893 candidates for $K_S^0 h^+ \pi^-$, 28589 for $K^+ h^- \pi^0$, and 9339 for $K_S^0 h^+ \pi^0$. To extract signal yields, we perform unbinned maximum likelihood fits using the observables M , ΔE , \mathcal{F} , $\cos \theta_B$, and the dE/dx of the faster of the two primary tracks (typically with momentum above 1 GeV/ c) in $K_S^0 h^+ \pi^-$ and $K^+ h^- \pi^0$ and of the only primary track in $K_S^0 h^+ \pi^0$. At high momentum, charged pions and kaons are statistically separated by their dE/dx and by ΔE , each of which provides discrimination at the 2.0σ level (1.7σ for CLEO II), and we fit for both particle hypotheses simultaneously. Charged pions and kaons with momentum below 1 GeV/ c are cleanly identified by dE/dx consistency at the 3σ level.

We perform one fit for each topology, $K_S^0 h^+ \pi^-$, $K^+ h^- \pi^0$, and $K_S^0 h^+ \pi^0$, allowing for six signal and background components, pion and kaon hypotheses for h^\pm for each of the following: signal, continuum background, and background from $b \rightarrow c$ decays. The probability for an event to be consistent with a given component is the product of the probability distribution function (PDF) values for each of the input variables (neglecting correlations). The likelihood for each event is the sum of probabilities over the six components, with relative weights determined by maximizing the total likelihood of the sample, which is given by the following

expression: $\mathcal{L} = \prod_{i=1}^{\#\text{events}} \left[\sum_{j=1}^{\#\text{components}} \left(f_j \prod_{k=1}^{\#\text{variables}} \mathcal{P}_{ijk} \right) \right]$. The \mathcal{P}_{ijk} are the per event PDF values, and the f_j are the free parameters optimized by the fit and constrained to sum to unity. Since the PDFs are normalized to unit integral over the fiducial region, the f_j can be interpreted as component fractions. The parameters of the dE/dx PDFs are measured from $D \rightarrow K^+\pi^-$ decays in data. For all other variables, the signal and $b \rightarrow c$ PDFs are determined from high-statistics Monte Carlo samples, and the continuum PDFs are determined from data collected below the $B\bar{B}$ production threshold. The impact of correlations among the input variables is reduced by determining the PDFs as a function of the event location in the Dalitz plot, for coarse bins in the $M^2(K\pi)$ - $M^2(\pi\pi)$ plane. We use Monte Carlo simulation to estimate the systematic error associated with neglecting any remaining correlations.

Detection efficiencies and crossfeed among the signal modes are measured from Monte Carlo simulated events. The statistical significance of the raw yield N reported by the fit is determined by repeating the fit with N fixed to be zero. A significance of $n\sigma$ results in an increase in $-2\ln\mathcal{L}$ of n^2 . We calculate fit yield upper limits (N^{UL}) at the 90% confidence level by integrating the likelihood function: $\frac{\int_0^{N^{UL}} \mathcal{L}_{\max}(N)dN}{\int_0^\infty \mathcal{L}_{\max}(N)dN} = 0.90$, where $\mathcal{L}_{\max}(N)$ is the maximum likelihood at fixed N , which conservatively accounts for possible correlations among the free parameters in the fit.

Table I lists the results of the fits to the three topologies. We observe a signal for $B \rightarrow K_S^0\pi^+\pi^-$ with a statistical significance of 8.1σ . Since the efficiency depends on position in the Dalitz plot, we evaluate the efficiency in bins across the Dalitz plot and apply a correction to each event. The branching fractions and upper limits thus obtained are free from model dependence. The efficiencies given in Table I are averages over the efficiencies for the observed events weighted by the probability that they are signal. For modes with yields consistent with zero, *i.e.* the three $KK\pi$ modes, the signal Dalitz plot distribution is unknown. Therefore, we examine several models of signal distribution across the Dalitz plot, both resonant and non-resonant, and we adopt the model with the lowest measured efficiency to establish conservative upper limits. The two sets of errors correspond to the statistical and systematic uncertainties, respectively. The largest contributions to the latter are uncertainties in the PDF parameters and reconstruction efficiencies. Branching fraction upper limits are increased by one standard deviation of the relative systematic uncertainty. We assume equal branching fractions for $\Upsilon(4S) \rightarrow B^0\bar{B}^0$ and B^+B^- , which is consistent with a recent measurement [13].

In these six-component fits, we measure yields for the three-body final states ignoring any possible resonant substructure. We also perform fits for each topology that include the Dalitz plot variables as inputs and allow for various intermediate resonances ($K^*(892)$, $K_0^*(1430)$, $\rho(770)$, and $f_0(980)$) as well as non-resonant phase space decay. The Dalitz plot PDFs include our knowledge of the helicity structure in these decays. We neglect interference among these processes and assign a systematic error estimated from Monte Carlo simulation. The decays $B \rightarrow K^+(X)h^-$, where $K^+(X)$ denotes $K^{*+}(892)$ or $K_0^{*+}(1430)$, are accessible through different $K^+(X)$ submodes in both the $K_S^0h^+\pi^-$ and $K^+h^-\pi^0$ topologies. To maximize our sensitivity to these decays, we perform the Dalitz plot fits for these two topologies simultaneously, with the branching fraction for each $K^+(X)h^-$ decay constrained to be equal in its two $K^+(X)$ submodes, which are related by isospin.

We perform Dalitz plot fits for the three topologies with differing combinations of in-

intermediate resonant and non-resonant states, with up to nine signal components. The only channel where we observe a statistically significant signal is $B \rightarrow K^{*+}(892)\pi^-$ with a yield of $12.6_{-3.9}^{+4.6}$ for $K^{*+}(892) \rightarrow K^0\pi^+$ and $6.1_{-1.9}^{+2.2}$ for $K^{*+}(892) \rightarrow K^+\pi^0$ and a combined significance of 4.6σ . The size of the signal is insensitive to the choice of other resonances included in the fit. In the $K_S^0 h^+ \pi^-$ topology, we find the fractional yield $N(K^{*+}(892)\pi^-)/N(K_S^0\pi^+\pi^-)$ to be $0.20_{-0.07}^{+0.08}$, which is 7.4σ from unity. With efficiencies of 8.1% and 3.9% for $K^{*+}(892) \rightarrow K^0\pi^+$ and $K^+\pi^0$, respectively, we obtain a branching fraction of $\mathcal{B}(B \rightarrow K^{*+}(892)\pi^-) = (16_{-5}^{+6} \pm 2) \times 10^{-6}$. Most theoretical predictions [3] for this branching fraction lie in the range $(2-14) \times 10^{-6}$.

Figure 1 shows the event distributions in M and ΔE for modes where we claim an observation. The background in these plots has been suppressed with cuts on the ratios of signal and background likelihoods computed without M and ΔE respectively. Overlaid are the fit projections for the signal and background components, scaled by the efficiency of the likelihood ratio requirements (40–50% for $K^0\pi^+\pi^-$ and 70–80% for $K^{*+}(892)\pi^-$). Figure 2a and 2b show the $M(K^0\pi^+)$ and $M(\pi^+\pi^-)$ distributions for events in the $K_S^0 h^+ \pi^-$ fit satisfying a likelihood ratio requirement. Overlaid are the fit predictions for background, $B \rightarrow K^{*+}(892)\pi^-$, and all other signal modes combined. We define the helicity angle for $B \rightarrow K^{*+}(892)(K^0\pi^+)\pi^-$, θ_{hel} , to be the angle between the $K^{*+}(892)$ daughter π^+ direction in the $K^{*+}(892)$ rest frame and the $K^{*+}(892)$ direction in the B rest frame. Figure 2c shows the distribution of $\cos \theta_{\text{hel}}$ in the region $0.75 < M(K^0\pi^+) < 1.05$ GeV/ c^2 after subtracting all contributions except $B \rightarrow K^{*+}(892)\pi^-$, which are estimated from data collected below the $B\bar{B}$ production threshold and from Monte Carlo simulation. The data are consistent with the $\cos^2 \theta_{\text{hel}}$ dependence expected for a pseudoscalar-vector B decay and reflected in the overlaid fit projection.

In summary, we have observed the three-body decay $B \rightarrow K^0\pi^+\pi^-$ with a branching fraction $(50_{-9}^{+10} \pm 7) \times 10^{-6}$. A simultaneous analysis of the Dalitz plots for this decay and for $B \rightarrow K^+\pi^-\pi^0$ reveals the presence of $B \rightarrow K^{*+}(892)\pi^-$ with a branching fraction $(16_{-5}^{+6} \pm 2) \times 10^{-6}$, which is larger than but consistent with most theoretical predictions.

TABLE I. Maximum likelihood fit results for three-body decays. Reconstruction efficiencies include all daughter branching fractions. The errors on branching fractions \mathcal{B} are statistical and systematic. Upper limits are computed at the 90% confidence level.

Mode	Raw Yield N	Significance	ϵ (%)	$\mathcal{B} \times 10^6$
$K^0\pi^+\pi^-$	$60.2_{-10.6}^{+11.5}$	8.1σ	12	$50_{-9}^{+10} \pm 7$
$K^0K^-\pi^+$	$2.4_{-2.4}^{+7.1}$	0.4σ	8.0	< 21
$K^+\pi^-\pi^0$	$43.0_{-13.5}^{+14.5}$	3.7σ	19	< 40
$K^+K^-\pi^0$	$0.0_{-0.0}^{+11.5}$	0.0σ	14	< 19
$K^0\pi^+\pi^0$	$20.3_{-8.8}^{+10.1}$	2.7σ	6.8	< 66
$K^0K^-\pi^0$	$0.0_{-0.0}^{+3.7}$	0.0σ	3.7	< 24

ACKNOWLEDGMENTS

We thank Matthias Neubert and Alex Kagan for useful discussions. We gratefully acknowledge the effort of the CESR staff in providing us with excellent luminosity and running conditions. This work was supported by the National Science Foundation, the U.S. Department of Energy, the Research Corporation, and the Texas Advanced Research Program.

REFERENCES

- [1] CLEO Collaboration, C. P. Jessop *et al.*, Phys. Rev. Lett. **85**, 2881 (2000); CLEO Collaboration, D. Cronin-Hennessy *et al.*, Phys. Rev. Lett. **85**, 515 (2000); CLEO Collaboration, S. J. Richichi *et al.*, Phys. Rev. Lett. **85**, 520 (2000); CLEO Collaboration, R. A. Briere *et al.*, Phys. Rev. Lett. **86**, 3718 (2001); Belle Collaboration, K. Abe *et al.*, Phys. Lett. B **517**, 309 (2001); A. Bozek for the Belle Collaboration, [hep-ex/0104041](#); Belle Collaboration, K. Abe *et al.*, Phys. Rev. Lett. **87**, 101801 (2001); BABAR Collaboration, B. Aubert *et al.*, [hep-ex/0109007](#); BABAR Collaboration, B. Aubert *et al.*, Phys. Rev. Lett. **87**, 151801 (2001); BABAR Collaboration, B. Aubert *et al.*, Phys. Rev. Lett. **87**, 151802 (2001); BABAR Collaboration, B. Aubert *et al.*, Phys. Rev. Lett. **87**, 221802 (2001); Belle Collaboration, K. Abe *et al.*, Phys. Rev. D **65**, 092005 (2002).
- [2] M. Kobayashi and T. Maskawa, Prog. Theor. Phys. **49**, 652 (1973).
- [3] L. L. Chau, H. Y. Cheng, W. K. Sze, H. Yao and B. Tseng, Phys. Rev. D **43**, 2176 (1991); A. S. Dighe, M. Gronau and J. L. Rosner, Phys. Rev. D **57**, 1783 (1998); M. Ciuchini, R. Contino, E. Franco, G. Martinelli and L. Silvestrini, Nucl. Phys. B **512**, 3 (1998); N. G. Deshpande, B. Dutta and S. Oh, Phys. Lett. B **473**, 141 (2000); A. Ali, G. Kramer and C. D. Lü, Phys. Rev. D **58**, 094009 (1998); M. Gronau and J. L. Rosner, Phys. Rev. D **61**, 073008 (2000); J. L. Rosner, Nucl. Instrum. Meth. A **462**, 44 (2001); C. W. Chiang and J. L. Rosner, Phys. Rev. D **65**, 074035 (2002); Y. -Y. Keum, H. Li, and A. I. Sanda, [hep-ph/0201103](#); D. Du *et al.*, [hep-ph/0201253](#); V. Chernyak, [hep-ph/0102217](#).
- [4] N. G. Deshpande, G. Eilam, X. G. He and J. Trampetic, Phys. Rev. D **52**, 5354 (1995); B. Bajc, S. Fajfer, R. J. Oakes, T. N. Pham and S. Prelovsek, Phys. Lett. B **447**, 313 (1999); S. Fajfer, R. J. Oakes and T. N. Pham, Phys. Rev. D **60**, 054029 (1999); A. Deandrea, R. Gatto, M. Ladisa, G. Nardulli and P. Santorelli, Phys. Rev. D **62**, 036001 (2000); A. Deandrea, R. Gatto, M. Ladisa, G. Nardulli and P. Santorelli, Phys. Rev. D **62**, 114011 (2000); A. Deandrea and A. D. Polosa, Phys. Rev. Lett. **86**, 216 (2001); S. Fajfer, R. J. Oakes and T. N. Pham, [hep-ph/0203072](#); H. -Y. Cheng and K. -C. Yang, [hep-ph/0205133](#); N. G. Deshpande, N. Sinha, and R. Sinha, [hep-ph/0207257](#).
- [5] Y. Gao and F. Würthwein (for the CLEO Collaboration), [hep-ex/9904008](#); CLEO Collaboration, C. P. Jessop *et al.*, Phys. Rev. Lett. **85**, 2881 (2000).
- [6] Belle Collaboration, K. Abe *et al.*, BELLE-CONF-0115 (2001), contributed to the Proceedings of the XX International Symposium on Lepton and Photon Interactions at High Energies, July 23-28, 2001, Rome, Italy; T. J. Gershon (for the Belle Collaboration), [hep-ex/0205033](#); H. C. Huang (for the Belle Collaboration), [hep-ex/0205062](#).
- [7] CLEO Collaboration, Y. Kubota *et al.*, Nucl. Instrum Methods Phys. Res. A **320**, 66 (1992).
- [8] T. S. Hill, Nucl. Instrum. Methods Phys. Res. A **418**, 32 (1998).
- [9] R. Brun *et al.*, CERN DD/EE/84-1.
- [10] S. L. Wu, Phys. Rep. C**107**, 59 (1984).
- [11] CLEO Collaboration, D. Asner *et al.*, Phys. Rev. D**53**, 1039 (1996).
- [12] G. Fox and S. Wolfram, Phys. Rev. Lett. **41**, 1581 (1978).
- [13] CLEO Collaboration, J. P. Alexander *et al.*, Phys. Rev. Lett. **86**, 2737 (2001).

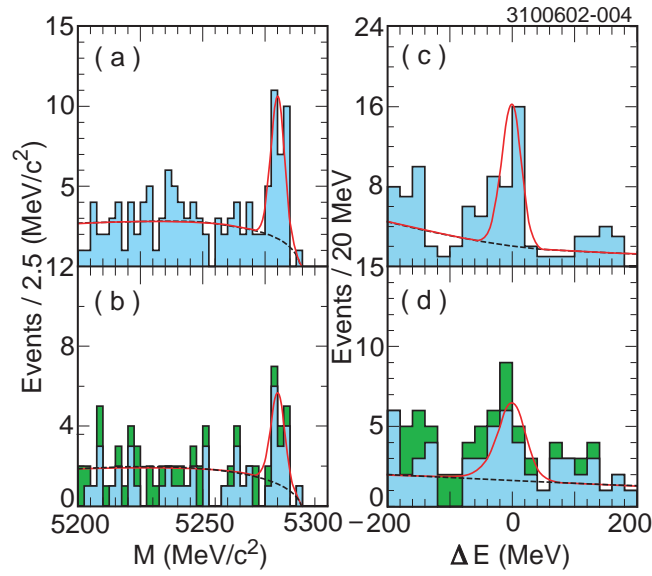


FIG. 1. M and ΔE projections for $B \rightarrow K^0\pi^+\pi^-$ (a and c) and $B \rightarrow K^{*+}(892)\pi^-$ (b and d), which include the two $K^{*+}(892)$ submodes, $K^{*+}(892) \rightarrow K^0\pi^+$ (light shade) and $K^{*+}(892) \rightarrow K^+\pi^0$ (dark shade). The background has been suppressed with cuts on the ratios of signal and background likelihoods computed without the displayed variable. The dashed and solid lines show the fit predictions for background and the sum of signal and background, respectively.

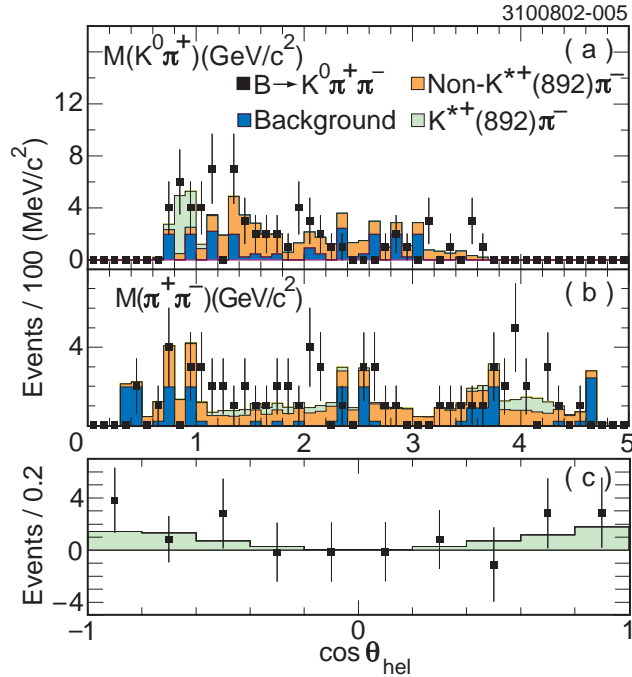


FIG. 2. $M(K^0\pi^+)$ and $M(\pi^+\pi^-)$ projections for $B \rightarrow K^0\pi^+\pi^-$ (a and b, respectively) and the $\cos\theta_{\text{hel}}$ projection for $B \rightarrow K^{*+}(892)(K^0\pi^+)\pi^-$ (c). Shown in (a) and (b) are the distribution for data (points) and the fit predictions for background (dark shade), the sum of all signal B decays except $B \rightarrow K^{*+}(892)\pi^-$ (medium shade), and $B \rightarrow K^{*+}(892)\pi^-$ (light shade). Shown in (c) are the data distribution (points) in the region $0.75 < M(K^0\pi^+) < 1.05 \text{ GeV}/c^2$ with all non- $K^{*+}(892)\pi^-$ contributions subtracted and the fit prediction for $B \rightarrow K^{*+}(892)\pi^-$ (histogram). The background has been suppressed with a cut on the ratio of signal and background likelihoods computed without the Dalitz plot variables.